Quantitative texture analysis of glaucophanite deformed under eclogite facies conditions (Sesia-Lanzo Zone, Western Alps): comparison between X-ray and neutron diffraction analysis

M. ZUCALI[1], D. CHATEIGNER[2], M. DUGNANI[1], L. LUTTEROTTI[3] & B. OULADDIAF[4]

[1]*Dipartimento di Scienze della Terra, Università di Milano, Via Mangiagalli 34, I-20133 Milano, Italy (e-mail: Michele.Zucali@unimi.it)*

[2]*Laboratoire CRISMAT-ISMRA, bd. M. Juin, 14050 Caen, France*[3]

Dipartimento di Ingegneria dei Materiali, Università degli Studi di Trento, Via Mesiano 77, I-38050 Trento, Italy

[4]*Institut Laue-Langevin, Neutron for Science, Rue Jules Horowitz 6, BP 156, F-38042 Grenoble Cedex 9, France*

Abstract: X-ray and neutron diffraction techniques have been applied to quantitative texture analysis of a glaucophanite from the Sesia-Lanzo Zone (Western Italian Alps), naturally deformed under eclogite facies conditions. The comparison has been carried out in order to reveal the limits and problems of texture analysis related to strongly deformed polymineralic. Different methods of measuring and computing the orientation distribution function from diffraction data have been tested, in particular X-rays, direct peak integration, and neutron diffraction using Rietveld-texture analysis. Due to grain-size problems and heterogeneity of individual amphibole minerals, neutron radiation is shown to be the best probe for characterizing the whole rock: being more penetrative than conventional X-rays, a larger volume of the mineral aggregate is sampled, giving better statistics. However, results obtained by summing the corresponding individual spectra of at least three X-ray diffraction experiments on parallel slabs of the same specimen also give statistically valid, semi-quantitative results that reproduce the overall textures. The quantitative texture analysis shows the strong texture of the two generations of amphiboles (AmpI and AmpII), which are mainly characterized by [001]*-directions at an angle of about 10° to the mineral lineation and by (*hk0*) planes describing girdles around the lineation. The texture is comparable to those described in the literature for amphibole deformed under different temperature and pressure conditions, and the pronounced asymmetry of the [001]* directions with respect to the mineral lineation is consistent with a non-coaxial component that occurs during the deformation.

In the recent past, quantitative texture analysis has been used in incredibly diverse applications in Earth Sciences (Wenk 1985; Bunge *et al.*1994; Kocks *et al.* 1998; Leiss *et al.* 2000). For instance in structural geology, tectonics, deformation processes and glaciology, texture analysis can be used to describe the anisotropy of fabrics (Baker *et al.* 1969; Baker & Wenk 1972; Gapais & Brun 1981; Bennet *et al.*1997; Leiss *et al.* 2000). In palaeontology, texture analysis brings new insights in to the phylogeny of molluscs and fossils (Chateigner *et al.* 2000). In geophysics, texture analysis aids interpretation of the anisotropic seismic wave propagation in the Earth's inner core (Wenk *et al.* 2000). Several techniques have been used to carry out texture analysis: the former optical U-stage has progressively been complimented by X-ray and neutron diffraction experiments, and more recently by the local electron back scattering diffraction approach (e.g., Prior *et al.*1999). In the case of X-ray and neutron diffraction, photographic films have rapidly been replaced by point detectors which have allowed the first real quantitative texture analyses by measuring diffraction pole figures. However, such detectors only measure one pole figure at a time and do not allow the separation of several textures in multiphase samples of the type commonly present in geological settings.

Bunge *et al.* (1982) proposed using neutrons to overcome the multiphase problem in texture analysis. Recently, Ricote & Chateigner (1999) used X-rays in which several pole figures were simultaneously acquired by use of a curved position sensitive detector. So far, however, quantitative texture studies of rocks composed of more than one phase of low crystal symmetry are rare

From: DE MEER, S., DRURY, M. R., DE BRESSER, J. H. P. & PENNOCK, G. M. (eds) 2002. *Deformation Mechanisms, Rheology and Tectonics: Current Status and Future Perspectives*. Geological Society, London, Special Publications, **200**, 239–253. 0305-8719/02/$15

(Siegesmund *et al.*1994; Wenk *et al.* 2000; Wenk *et al.* 2001).

Microstructural investigations, using optical microscopy, X-ray and neutron diffraction, scanning electron and transmission electron microscopy show that (100)[001] and (*hk0*)[001] are the most common slip systems in amphiboles (Table 1). Dynamic recrystallization (Cumbest *et al.* 1989), rigid body rotation (Ildefonse *et al.* 1990; Siegesmund *et al.* 1994) and cataclastic deformation (Nyman *et al.* 1992) may also occur. The most frequently recurrent amphibole textures consist of [001]-direction and (*hk*0) planes parallel to the stretching lineation (e.g., Schwerdtner 1964; Gapais & Brun 1981; Siegesmund *et al.* 1994). These studies also showed that the roles of intracrystalline plasticity, fracture, rigid body rotation and chemical forces

Table 1. *Deformation mechanisms in naturally and experimentally deformed amphiboles reported in the literature*

References	Deformation conditions	Observation techniques	*P–T* conditions	Mineral	Deformation mechanisms, slip systems and twin systems
Schwerdtner (1964); Schwerdtner *et al.* (1971)	NAT	OM		Hbl	stress-driven growth: [001] maxima perpendicular to {110} girdle
Riecker & Rooney (1969); Rooney *et al.* (1970)	EXP	OM-XR	400–600 °C; 5–15 kbar	Hbl	(100) (−101) twinning
Dollinger & Blacic (1975)	EXP/NAT	OM	AMP <800 °C >800 °C GS	Hbl Act	(100)[001] (100) variable directions (100)[001]
Kern & Fakhimi (1975)	EXP	XR	20–700 °C at 2kbar	Hbl	[110]//XZ planes of fabric and [001] deduced// lineation
Morrison 1976					
Gapais & Brun (1981)	NAT	XR	IP-LP/HT	Hbl	[001] // lineation
Biermann (1981)	NAT	—	—	—	(100) twinning
Biermann & Van Roermund, (1983)	NAT	OM TEM	450–600 °C 4–6 kbar	Clino-Amp	(hk0)[001]
Cumbest *et al.* (1989)	NAT	OM TEM	AMP	Hbl Clino-Amp	Dynamic re-crystallization (core-mantle microstructure)
Mainprice & Nicolas (1989)	NAT	OM-XR-TEM		hbl	[001]//lineation
Reynard *et al.* (1989)	NAT	TEM	ECL	Gln	(100)[001] {110}[001] (010)[100] {110}1/2⟨1−10⟩ (001)1/2⟨110⟩
Ildefonse *et al.* (1990)	NAT	OM	ECL	Gln	Rigid body rotation
Skrotzki (1990; 1992)	NAT	TEM	$T > 650$ °C	Hbl	(100)[001]
Krhul & Huntemann (1991)	NAT		GR	Hbl	[001]//lineation
Nyman *et al.* (1992)	NAT	OM SEM TEM	~500 °C 3–5 kbar	Hbl	Cataclastic deformation
Shelley, (1992; 1994; 1995)	NAT	OM	BS	Hbl	anisoptropic growth (or solution); [001]//lineation
Siegesmund *et al.* (1994)	NAT	OM ND	AMP	Hbl	Rigid body rotation or dynamic recrystallization
Berger & Stünitz (1996)	NAT	OM TEM	500–670 °C >4 kbar	Hbl	Rigid body rotation

NAT, naturally deformed; EXP, experimentally deformed; OM, optical microscopy; XR, X-ray; TEM, transmission electron microscopy; ND, neutron diffraction; AMP, amphibolite facies; GS, greenschists facies; BS, blueschist facies; ECL, eclogite facies; GR, granulite facies; Hbl, hornblende; Act, actinolite; Amp, amphibole; Gln, glaucophane.

during the deformation of amphiboles under different geological conditions, need more quantitative investigation.

Needs clarification?

Neutron diffraction is well known as the most reliable experimental technique for quantitative texture analysis (QTA) of naturally deformed rocks where statistics, in coarse-grained samples, is a big concern (Bouchez *et al.* 1979; Wenk *et al.* 1984; Kocks *et al.* 1998; Chateigner *et al.* 1999). X-ray diffraction suffers from poor statistics when the grain size is not very fine, as is the case in many geological situations. This work first investigates the possibility of using the X-ray diffraction method to achieve a better reliability at least for qualitative results. Secondly, we compare two different methodologies of analysis with respect to their applicability to more complex polymineralic rocks. Finally, amphibole textures obtained with X-ray and neutron diffraction techniques are compared with microstructural features and crystallographic orientations reported in literature.

Geological setting and sample description

The M26 sample is a glaucophanite, mainly constituted of winchitic amphiboles (≥97%) (Table 2). It crops out along the divide between Monte Mucrone and Mombarone, in the Eclogitic Micaschists Complex (EMC) of the Sesia-Lanzo Zone (Austroalpine domain – Western Alps, Italy) (Fig. 1). This zone consists of two main tectonic units distinguished on the base of their lithological and metamorphic differences (e.g. Compagnoni 1977): the upper unit (II Zona Diorito-Kinzigitica) and the lower unit (Gneiss Minuti Complex and the EMC). The EMC shows a dominant Alpine imprint under eclogite facies conditions. The EMC consists of small lenses of biotite–garnet–Al silicates–metapelites (kinzigites), garnet–omphacite–glaucophane–metapelites, large omphacite–glaucophane–metaquartzdiorite bodies (metagranitoids and metaquartzdiorite of Monte Mars Complex, western part of the Monte Mucrone intrusion emplaced at 293 ± 1 Ma (Bussy *et al.* 1998)), lenses of metabasites (amphibole-bearing eclogites, eclogites and glaucophanites), pure and impure marbles, kyanite–chloritoid–garnet–quartzites, metre-size peridotitic lenses and andesitic dykes (Gosso 1977; Pognante *et al.* 1980; Passchier *et al.* 1981; Spalla *et al.* 1983; Williams & Compagnoni 1983; Lardeaux & Spalla 1991; Venturini *et al.* 1991). All lithologies, except Oligocene andesitic dykes (Dal Piaz *et al.* 1979; De Capitani *et al.* 1979; Beccaluva *et al.* 1983) show a penetrative structural and metamorphic Alpine re-equilibration under eclogite facies conditions. The age of the eclogitic metamorphism has been dated as Late Cretaceous–Early Paleocene (Inger *et al.* 1996; Duchene *et al.* 1997; Ruffet *et al.* 1997; Rubatto *et al.* 1999).

The structural framework of the EMC, along the Monte Mucrone–Mombarone divide, is the result of seven deformation phases (Pognante *et al.* 1980; Passchier *et al.* 1981; Williams & Compagnoni 1983). The most penetrative is D_2; it consists, within micaschists and gneisses, of a penetrative foliation (S2, 265°/40°) marked by eclogite facies minerals, as omphacite, blue-amphibole and phengite; in eclogites, amphibole-bearing eclogites and glaucophanites, D_2 mainly consists of an S_2 foliation, defined by a compositional layering associated with a mineral lineation (L_2, 250°/35°); the latter lineation (L_2) is defined by shape preferred orientation of omphacite and glaucophane. Subsequent deformation phases (D_3 and D_4) produced large-scale isoclinal and recumbent folds. Glaucophanites are metre-scale lenses or boudins within eclogitic micaschists and gneisses; they are characterized by centimetre to millimetre scale grain size variations. The macroscopic lineation (L_2) lies within the S_2 compositional layering and is marked by the shape preferred orientation of glaucophanes and by the preferred orientation of lenticular aggregates of glaucophanes (Fig. 2). No syn-D_2 fabric gradients occur at the mesoscopic scale within the glaucophanites and surrounding micaschists and gneisses. The

Table 2. *Chemical analyses of M26 amphiboles*

	AmpI	AmpII	AmpIII
SiO_2	59.717	59.658	57.343
TiO_2	0.111	0.043	0.101
Al_2O_3	**12.112**	**11.946**	**2.009**
FeO	6.163	6.303	5.801
MnO	0.097	0.000	0.099
MgO	13.406	13.453	19.993
CaO	2.111	2.166	13.254
K_2O	0.064	0.000	0.075
Na_2O	**4.512**	**4.906**	**0.162**
Total	98.293	98.475	98.837
Si	7.945	8.035	7.875
Ti	0.008	0.008	0.008
Al	1.899	1.895	0.322
Fetot	0.690	0.707	0.669
Mn	0.008	0.000	0.008
Mg	**2.661**	**2.701**	**4.095**
Ca	**0.299**	**0.316**	**1.949**
K	0.008	0.000	0.017
Na	1.160	1.280	0.041

Stoichiometric ratios of elements based on 23 O. Fetot as Fe^{2+}.

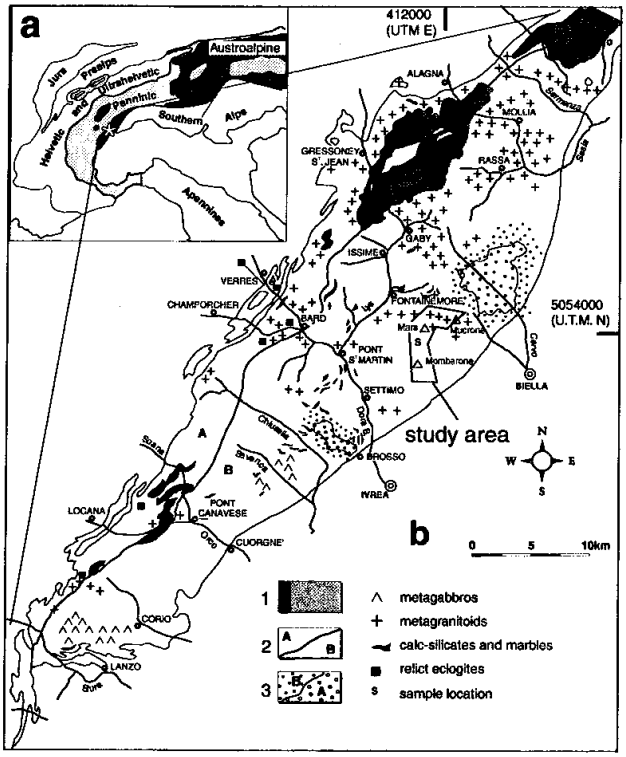

Fig. 1. (a) Tectonic outline of the Alpine Chain. A star identifies the Sesia-Lanzo Zone. (b) Simplified geological map of the Sesia-Lanzo Zone. 1, II Zona Diorito-Kinzigitica; 2A, Gneiss Minuti Complex (GMC); 2B, Eclogitic Micaschists Complex (EMC); 3A, non-metamorphic Tertiary intrusives; 3B, contact metamorphic aureole.

glaucophanite has been sampled where minor overprinting by subsequent deformation and metamorphic transformations occurred (e.g. D_3 and D_4 folds).

Thin sections for optical microscopy were cut parallel to the mineral lineation (L_2) and perpendicular to the foliation S_2 (XZ plane in Fig. 2). Glaucophanite exhibits a compositional layering defined by alternating domains ($\leq$5 mm thick). Domains I have a lenticular shape; large AmpI occur as ellipsoidal grains (0.4–1 mm) within domains I, showing undulose extinction, deformation bands and in some places subgrains (Fig. 2). Domains I are discontinuous, and wrapped by domains II, parallel to S_2. AmpI grains do not have a shape preferred orientation with respect to S_2 and L_2. AmpI porphiroclasts, displaying undulose extinction and marginal subgrains, occur in the core of the domains I. The misorientation angle between adjacent subgrains is often higher than 5° (Fig. 2). Subgrains at the rims of the domains I display shape preferred orientation close to S_2 and L_2 directions. Domains II are defined by aggregates of AmpII. AmpII are mainly strain free with grain sizes <0.4 mm. Shape preferred orientation of AmpII is parallel to the mineral layering (S_2) (Fig. 2a) and the AmpII grains are similar in size to AmpI marginal subgrains. AmpI shows rutile, zircon, opaques and quartz inclusions. A third generation of amphibole (AmpIII) occurs locally at the grain boundaries between amphiboles (Fig. 2). Chlorite and white mica partially replace AmpI and AmpII or fill small fractures with quartz and carbonates. Garnet appears as small porphyroblasts ($\leq$1 mm) and forms less

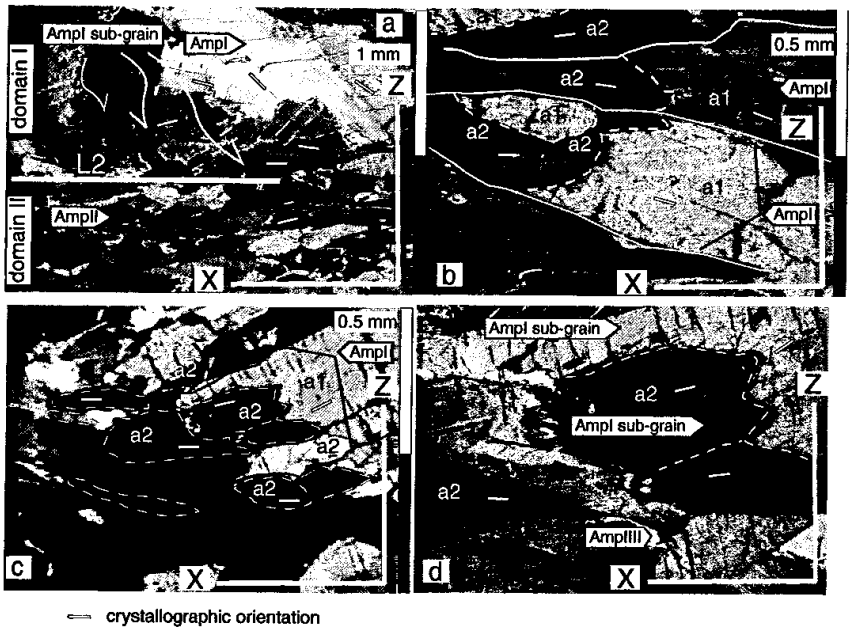

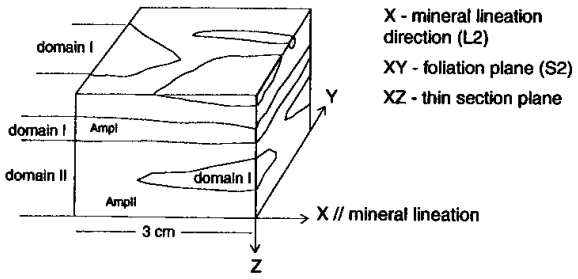

Fig. 2. (**a**) Alternating domains I and II, marking the mineralogical lineation (L_2). Domain I is defined by an elongated aggregate of AmpI with no shape preferred orientation; domain II is defined by shape preferred orientation of AmpII grains, elongated parallel to the mineral lineation (L_2). AmpI subgrains at the domain boundary show shape preferred orientation parallel to L_2. (**b**) Continuous white and black lines define the AmpI grain boundaries, while stippled white lines define AmpI subgrain boundaries; *a1* grains preserve shape and crystallographic orientation of AmpI; *a2* sub-grains show different degrees of misorientation with respect to AmpI crystal orientation. (**c**) and (**d**) AmpI, within domain I, with elongate strain free subgrains (*a2*); shape preferred orientations of subgrains mainly lie parallel to the X direction.

than 1% of the rock volume. Micro-fractures (2 mm thick), occurring at high angles (~90°) with respect to the layering, are mainly filled by fine aggregates of quartz, carbonates, diopside and white mica.

Mineral chemistry and quantitative diffraction analyses

Quantitative chemical analyses were performed on polished samples using an Applied Research

Laboratories electron microprobe fitted with six wavelength-dispersed spectrometers and a Tracor Northern Energy Dispersive Spectrometer 5600, using natural silicates as standards. An accelerating voltage of 15 kV, a sample current 20 nA and a beam current 300 nA were used. Matrix corrections were calculated using the ZAF procedure (Colby 1968). Table 2 shows representative mineral compositions of AmpI, AmpII and AmpIII. While AmpI and AmpII display the same chemical composition (winchite), AmpIII (actinolite) is characterized by a decrease in Al and Na content and an increase of Mg and Ca content.

A representative sample of M26 glaucophanite (1 cm^3) was powdered with an agate mortar and a powder diffraction pattern was collected using Cu Kα radiation, from 5° to 70°, in steps of 0.01° and 3 seconds per step. A quantitative phase analysis using the Rietveld method was performed using a richterite (Hawtorn *et al.* 1997) and a clinochlore (Smyth *et al.* 1981) as starting structural models. The atomic fractions were deduced from chemical analysis. The quantitative phase analysis confirmed that the total amount of chlorite and AmpIII is less than 5%. The other phases, observed using optical microscopy, are below the detection limits of the X-rays.

Texture measurements

Measuring single pole figures does not allow a quantitative texture analysis, even when measured completely; in order to compare between samples independently (e.g. porosity, stress/strain states, particle sizes and phase ratios) normalization of pole figures is needed (Bunge & Esling 1982). Normalization involves refining the orientation distribution function (ODF), which defines the texture strength and all components of the texture. The same single pole figure can be generated by many different ODFs, which means that interpretation of texture from a single pole figure is ambiguous.

X-ray diffraction

X-ray diffraction texture measurements were carried out using a Huber four-circle goniometer (closed eulerian cradle $+\theta$–2θ movements) mounted on an INEL X-ray generator, and Cu Kα wavelength radiation, monochromatized by an incident flat graphite monochromator. A curved position sensitive detector (PSD) with a 2θ resolution of 0.03° (INEL CPS-120) was used to acquire complete diffraction patterns at different positions of the sample in the 0–120° 2θ range. The flat samples were measured in reflection geometry. The incident angle on the sample ω, and the PSD position were chosen to maximize coverage in orientation space. The spectra were measured using a coverage from 0° to 355° in φ and from 0° to 70° in χ (Fig. 3) with incremental steps of 5° for both angles, which corresponds to $72 \times 15 = 1080$ measured 2θ patterns. Each pattern was acquired for 180 seconds.

We chose an X-ray beam size of 1×1 mm, collimated to provide sufficient resolution for peak separation and for an average grain size of 0.1–0.4 mm; larger AmpI grains (0.5–0.8 mm) correspond to less than 2% of the sample. The irradiated surface was increased by oscillations of the sample perpendicular to the lineation direction (±3 mm of amplitude) (Fig. 3). A further increase of the irradiated area could be provided by lowering ω, but such a procedure would give rise to more severe peak overlap due to a defocusing effect, particularly at high 2θ values, where much of the orientation information is located. Compared to a set-up with a point detector, this experimental design allows an optimized incident angle value of $\omega = 16°$. To further increase the grain statistics, three slabs of the same sample, cut perpendicular to the mineral layers and parallel to the mineral lineation, were measured. The respective raw intensities for each pole figure direction obtained from the three different experiments were summed before the ODF calculation.

Figure 3a shows the sum of 1080 diagrams of M26 used for the phase identification and peak indexing at the $\omega = 16°$ position, and Fig. 3b is an example of such a summed diagram for a lower incidence angle ($\omega = 5.3°$). Such diagrams are close to random powder patterns, but only approximately since the pole figures were incompletely measured. The summed diagram confirms that the AmpI and AmpII chemical compositions are similar. The increased overlap for the lower ω value can be clearly seen (Fig. 3b), leading to unreliable integration for 2θ values larger than 40°. For this reason only the experiments at $\omega = 16°$ have been used. Indexing of the diagrams used shows that at least twenty pole figures are theoretically usable for the ODF determination. Some peaks are however weak, closer to the background counts, and these would decrease the overall reliability of the ODF; therefore, only thirteen have been used in the analysis, removing peaks lower than 8% of the maximum.

To obtain these pole figures for texture analysis, data treatment was operated through direct

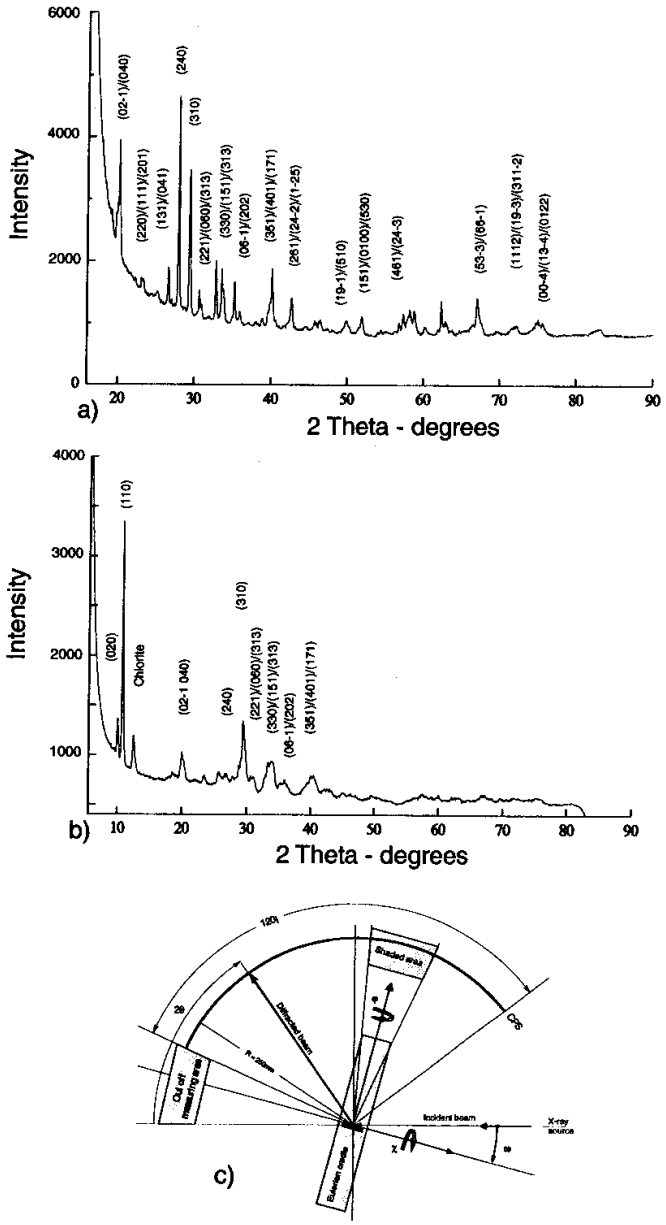

Fig. 3. Summed X-ray diffraction diagrams at 16° (**a**) and 5.3° (**b**) ω angles. (**c**) Instrument angles in reflection geometry.

Table 3. *Declared overlapping peaks for x-ray analysis, overlapping factors (%) and Chi ranges*

Miller indices			Declared Overlaps (%)	min Chi	max Chi
1	1	1	30	0	70
2	2	0	20	0	70
2	0	1	50	0	70
1	3	1	30	0	70
0	4	1	70	0	70
2	2	1	20	0	70
0	6	0	1	0	70
3	1	5	79	0	70
1	5	1	40	0	70
3	3	0	40	0	70
3	1	3	20	0	70
0	6	−1	50	0	70
2	0	2	50	0	70
3	5	1	70	0	70
4	0	1	15	0	70
1	7	1	15	0	70
2	6	1	5	0	70
2	4	−2	70	0	70
1	−2	5	25	0	70
1	9	−1	50	5	70
5	1	0	50	5	70
1	5	1	15	5	70
0	10	0	5	5	70
5	3	0	80	5	70
4	6	1	50	10	70
2	4	−3	50	10	70
5	3	−3	30	15	70
6	6	−1	70	15	70
1	11	2	50	20	70
1	9	−3	30	20	70
3	11	−2	20	20	70
0	0	−4	10	20	70
1	3	−4	50	20	70
0	12	2	40	20	70

cyclic integration of the diffracted intensities and corrections for absorption using an INEL-LPEC software program (INEL 1986). The WIMV (Matthies & Vinel 1982) iterative method was subsequently used to compute the ODF from the selected pole figures. The quality of the result was assessed with reliability factors (RP0 and RP1, for global and above 1 m.r.d., or multiple of random distribution, values respectively). From the ODF, we can recalculate any pole figures, even those that are not available experimentally, and calculate parameters indicative of the texture strength: the texture index (F^2), and the texture entropy (S) (after Bunge 1982; Matthies 1991).

The different calculations have been carried out using the Berkeley Texture Package (BEARTEX, Wenk *et al.* 1998). Depending on the sample composition several diffraction peaks coming from different phases can be present at close 2θ positions. For X-ray data analysis where only the direct integration method was used to obtain pole figures, we only used single peaks, or peak overlaps coming from the same phase as a summed multi-pole figure. The overlaps can be treated by the WIMV method, assigning intensity contributions to each component of the multi-pole figure (weight in % in Table 3).

Neutron diffraction

Neutron diffraction experiments were carried out at the Institut Laue-Langevin (ILL, Grenoble, France) high flux reactor using the position-sensitive detector of the D1B beamline. The detector spans a 2θ range of 80° with a resolution of 0.2° and the wavelength used was 2.523 Å. The sample (1 cm^3) was mounted in a transmission Debye-Scherrer geometry and measured with the same scan grid as for X-ray experiments, but the pole figure coverage extended to 90° in χ, thanks to the low absorption of neutrons in this type of material. The ω, value was 10° and the counting time was 50 seconds per spectrum. A total of $72 \times 19 = 1368$ measured scans over the accessible 2θ range were made. Figure 4a shows the summed neutron diffraction pattern of the M26 sample for the 1368 scans. Since no defocusing effect occurs in transmission geometry and the full χ range is measured, such a diagram is closer to a powder diffraction pattern than an X-ray diffraction pattern, even when a blind area exists for pole figures at $\theta \neq \omega$. The neutron diffraction pattern shows an agreement between AmpI and AmpII chemical compositions. The smaller range of 2θ values, due to the larger wavelength used, gave fewer peaks. The MIMA function of Beartex, a subroutine based on the Minimal Pole Density Set (MPDS) criterion (Helming 1991), was used to compute the minimum requirement in experimental data to fulfil the condition that any ODF cell is determined by at least three points coming from the experimental pole figures. MIMA results show that the orientation space was completely covered by both the X-ray and neutron data sets, allowing recalculation of the quantitative textures using the WIMV algorithm.

Numerical integration is not suitable for reliable ODF determination because of the relatively low 2θ resolution, and either a Rietveld texture analysis or a peak fit separation (Howard & Preston 1989) should be chosen to resolve the overlaps. The latter is, however, less capable of separating exact and/or strong overlaps than

Changes ok?

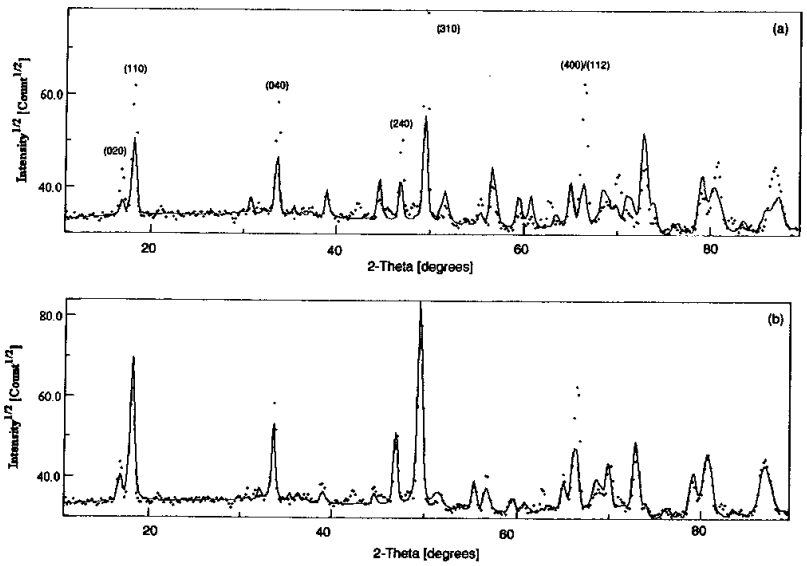

Fig. 4. **(a)** Neutron diffraction spectrum at $\varphi = 0°$ and $\chi = 60°$ after fitting by Maud, not considering texture. **(b)** Same spectrum as in **(a)** but considering texture. Crosses: measured data. Solid line: calculated pattern.

the Rietveld Texture analysis (Matthies *et al.* 1997). A Rietveld texture analysis (Lutterotti *et al.* 1997) was performed for all patterns with the software package MAUD (Lutterotti *et al.* 1999), considering amphibole as the only phase present. MAUD uses a Rietveld core routine to compute spectra and a so-called Le Bail algorithm (Matthies *et al.* 1997) to extract the differences between random and textured intensities for each computed peak. These spectra form the basis for computing the ODF using WIMV. Finally, the spectra were recomputed using the results from the ODF for the next Rietveld iteration step. Initially, lattice parameters (Table 4), a five-parameter background function, 2θ displacement of the peaks and the three-parameter Caglioti for the peak shape function, were simultaneously refined for five cycles assuming the sample was not textured. The discrepancy in fitting after these first steps suggests how strong the texture is (Fig. 4a). Then, the Le Bail-WIMV routines for the ODF computation were activated and texture was iteratively refined with crystal structure, yielding a better agreement between observed and calculated patterns (Fig. 4b). A first attempt to refine atomic positions as well as B_{iso} led to unusual values and these were replaced by values found in the literature for the next steps. Crystallographic results are compared with those of glaucophane (Comodi *et al.* 1991) and winchite (Ghose *et al.* 1986) in Table 4.

Should this be defined?

Table 4. *Lattice parameters for amphiboles*

Lattice parameters		Estimated standard deviation	Glaucophane (Comodi *et al.* 1991)	Winchite (Ghose *et al.* 1986)
a (Å)	9.5355	7.7517E-05	9.5310	9.7573
b (Å)	17.706	1.6669E-05	17.7590	17.9026
c (Å)	5.2823	7.1603E-05	5.3030	5.2886
beta (°)	103.78	8.1959E-05	103.59	103.81
Rw	0.1053	—		

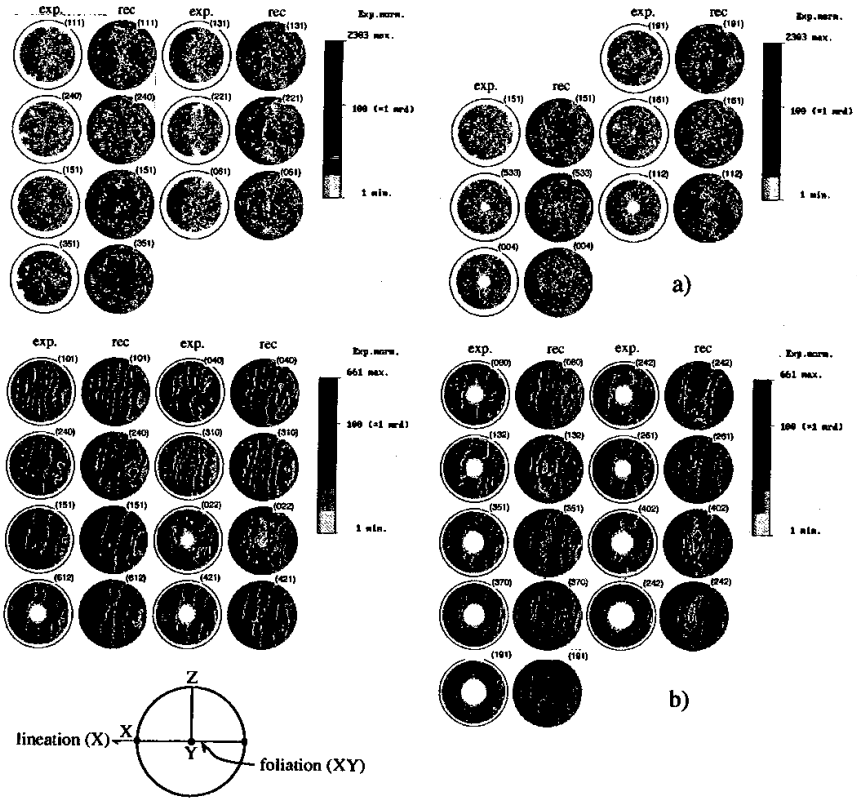

Fig. 5. Experimental normalized (exp.) and recalculated (rec.) X-ray (**a**) and neutron (**b**) pole figures for amphibole. Equal area projections. Logarithmic density scale. Intensity values are in m.r.d. ×100.

Results

Figure 5 shows the experimental normalized and recalculated pole figures from the X-ray and neutron analyses with respect to lineation direction and foliation plane. For X-rays, the high χ range was not completely covered and characteristic rings appear at unmeasured regions in recalculated pole figures (Fig. 5a). Such rings prove that, for the X-ray case, the MPDS is at the lower limit for the full ODF coverage.

X-ray pole figures (Fig. 5a) display symmetric and asymmetric girdles around mineral lineation for most pole figures (e.g. (111), (131), (240) and (221)). The quality assessment of the ODF is given by a comparison of the experimental and recalculated pole figures and by the RP0 and RP1 values in Table 5. We can clearly see in this case that the orientation density values are not as low as those revealed by neutrons. This is mainly due to the low grain statistics, which intrinsically force the WIMV algorithm to

Table 5. *Texture parameters after OD refinement from WIMV*

	X-ray pole figures	Neutron pole figures
Number of pole figures	13	17
OD minima (m.r.d.)	0.00	0.00
OD maxima (m.r.d.)	23.03	6.61
S	−2.91	−1.10
F^2 (m.r.d.^{2})	34.17	6.33
RP_0 averaged (%)	55.03	13.69
RP_1 averaged (%)	29.12	10.74

enhance the overall texture strength. However, these strong densities are obtained through an ODF refinement, the convergence of which ensures coherency between pole figures. A qualitative interpretation of the results is then made possible, with the grain-size problem affecting only the density values. Recalculated pole figures do not perfectly reproduce the experimental ones, as seen from the quite high RP factors. This is a consequence of the presence of some large grains. The strong amphibole texture is clearly shown by recalculating some special pole figures from the ODF focussing on principal crystal directions (Fig. 6a). The non-measurable $[001]^*$ directions are close to the lineation and $[010]^*$ and $[100]^*$ are mainly scattered within a plane perpendicular to the lineation direction. The $[001]^*$ directions make an angle lower than 10° with the lineation and display an angle of <15° with respect to XZ plane as shown by the asymmetry of maxima.

Similar features to those described above can also be observed in the neutron pole figures (Figs 5b and 6b). Here, experimental pole figures are smoother than those obtained with X-rays, and recalculated pole figures (Fig. 5b) closely reproduce the experimental ones, with corresponding lower RP values. Experimental and recalculated pole figures exhibit great and small circle distributions close or perpendicular to the lineation direction. As for the X-ray pole figures, a small angle between the lineation and $[001]^*$ directions is apparent, as shown by the low Miller indices pole figures (Fig. 6b). The $[001]^*$ directions are strongly oriented, with an angle slightly deviating from the lineation: approximately 10° and 15° with respect to the XZ plane. The $[010]^*$ and $[100]^*$ directions mainly describe maxima normal to the lineation direction.

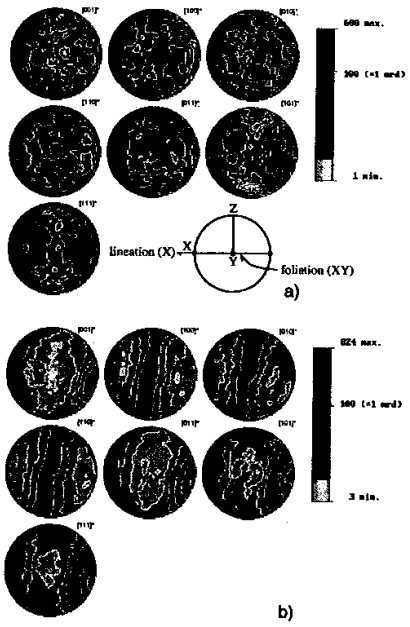

Fig. 6. X-ray (**a**) and neutron (**b**) pole figures recalculated with BEARTEX. Equal area projections. Logarithmic density scale. Intensity values are in m.r.d. ×100.

Discussion and conclusions

The M26 glaucophanite exhibits a strong texture, as shown by the pole density distribution of the amphibole and the texture indices reported in Table 5. The texture is comparable with those described in amphiboles deformed at different pressure and temperature conditions: the $[001]^*$ and $[110]^*$ directions mainly lie parallel and perpendicular to the lineation respectively (e.g., Schwerdtner 1964; Schwerdtner *et al.* 1971; Gapais & Brun 1981; Mainprice & Nicolas 1989; Kruhl & Huntemann 1991; Siegesmund *et al.* 1994), where the $[110]^*$ orientation is a function of the fabric components (Gapais & Brun 1981). In the M26 glaucophanites, $[100]^*$ and $[010]^*$ directions scatter within the YZ-plane of the strain ellipsoid, and $[001]^*$ directions lie at an angle with respect to the lineation and foliation. This can be interpreted as due to a dominant constrictional component of the finite strain (Gapais & Brun 1981). The asymmetry of the $[001]^*$ directions with respect to the fabric elements could be interpreted as having developed during a non-coaxial deformation (e.g., simple shear), as observed in other materials (Nicolas & Poirier 1976; Gapais & Cobbold 1987; Mainprice & Nicolas 1989; Law 1990; Wenk 1998). In the literature, the observed preferred orientations have been mainly interpreted as due to (100)[001] slip, rigid body rotation and oriented growth (see Table 1 for references). The crystallographic preferred orientations of the M26 sample suggest a strong influence of crystal shape, as shown by Ildefonse *et al.* (1990) for glaucophane within the Eclogitic Micaschists of the Sesia-Lanzo Zone and for hornblende in amphibolites where the weak matrix is constituted of plagioclase (Gapais & Brun 1981; Siegesmund *et al.* 1994). Our sample is matrix free, and

domains II, mainly constituted by AmpII, wrapping around domains I. Furthermore, AmpI porphyroclasts show undulose to patchy extinction, deformation bands and subgrains (Fig. 2). Subgrains in the core of the domains I show neither undulose extinction nor shape preferred orientations. Subgrains at the rims of the domains I progressively show a tendency to be oriented parallel to the domains II. The grain size and preferred orientation of such subgrains is similar to those of the AmpII defining domains II and both are mainly strain free. These relationships account for a component of subgrain rotation during the development of S2 and for AmpII-rich domains II having mechanically behaved as a 'weak matrix' with respect to the domains I (Cumbest *et al.* 1989; Siegesmund *et al.* 1994).

The relationships between the meso–microstructures and crystallographic textures, described above, do not unequivocally discriminate the dominant deformation mechanism during the development of the glaucophanite preferred orientation. In general, the nature of the deformation mechanisms leading to amphibole textures still remains incompletely resolved (e.g. Stünitz 1989; Siegesmund *et al.* 1994). Aside from these limitations, the present work shows that similar crystallographic textures occur in amphiboles deformed under amphibolite and eclogite facies conditions, except for the pronounced asymmetries of [001]* directions with respect to the fabric elements. Further investigations on other lithologies of the Sesia-Lanzo Zone, such as eclogitic micaschists or eclogites, may provide more quantitative textural data of the deeply subducted slice of continental crust in the Sesia-Lanzo Zone. Such data can be used to study the mechanical behaviour of rock-forming minerals during the important natural process of subduction to mantle depths and their relationships with whole rock deformation mechanisms.

The comparison of the two techniques shows that X-ray data can produce semi-quantitative results, which reproduce the overall texture if a sufficient area of the sample, or different sections of the same sample, are scanned using similar conditions. Neutron results are statistically more reliable (Table 5). The reliability of the different computation techniques is confirmed by the textures obtained: both direct peak integration (X-ray) and Rietveld texture analysis (neutron) produced qualitatively similar results even when starting from raw intensities obtained through different acquisition techniques (Ullemeyer *et al.* 2000), and agree with the results reported in the literature. However, it can be seen that, besides the comparatively limited accessibility of neutron experiments to users, the much larger resolution of X-rays using a PSD gives a high potentiality in QTA of geological samples of half-millimetre sized grains. The relatively poor 2θ resolution of thermal neutrons makes the separation of peaks from several phases a hard task, even with a Rietveld-like technique. This can be demonstrated, as in this work, by the strong correlation existing between fitted parameters such as atomic positions or isotropic Debye-Waller factors and texture coefficients, causing the refinements to diverge when all the parameters are refined. No atomic structure variations between samples can be accessed under these conditions, and with the resolution used, this limits the neutron applicability. X-rays offer a better resolution, but their lower χ measurable range illustrates another limitation. The use of a Rietveld texture methodology overcomes this limitation by increasing the number of pole figures used in the QTA analysis, together with a better atomic structure definition than that which is accessible from the better resolution. This methodology requires a high number of diffraction diagrams and a diffraction apparatus equipped with a position sensitive detector or area detector that can realize such measurements in a reasonable experimental time. Indeed, if the grain statistic problem is alleviated by special measuring practices, such as larger oscillations than those used in the present work, X-ray diffraction using the direct integration method suggests that a complete quantitative description of textures and structures of strongly polyphasic rocks can be achieved by implementing the X-ray Rietveld texture analysis.

The authors greatly thank G. Gosso, M. I. Spalla and G. Artioli from Università di Milano. The manuscript was improved through the very constructive reviews of D. Gapais and B. Leiss. The work was funded by COF. MURST 40% 1999.

References

Baker, D. W. & Wenk, H. R. 1972. Preferred orientation in a low-symmetry quartz mylonite. *Journal of Geology*, **80**, 81–105.

Baker, D. W., Wenk, H. R. & Christie, J. M. 1969. X-ray analysis of preferred orientation in fine-grained quartz aggregates. *Journal of Geology*, **77**, 144–172.

Beccaluva, L., Bigioggero, B. *et al.* 1983. Post-collisional orogenic dyke magmatism in the Alps. *Memorie della Società Geoligica Italiana*, **26**, 341–359.

BENNET, K., WENK, H.-R., DURHAM, W. B., STERN, L. A. & KIRBY, S. H. 1997. Preferred crystallographic orientation in the ice I > II transformation and the flow of ice II. *Philosophical Magazine*, **A76**, 413–435.

BERGER, A. & STUNITZ, H. 1996. Deformation mechanism and reaction of hornblende: examples from the Bergell tonalite (Central Alps). *Tectonophysics*, **257**, 149–174.

BIERMANN, C. 1981. (100) deformation twins in naturally deformed amphiboles. *Nature*, **292**, 821–823.

BIERMANN, C. & VAN ROERMUND, H. L. M. 1983. Defect structures in naturally deformed amphiboles – a TEM study. *Tectonophysics*, **95**, 267–278.

BOUCHEZ, J. L., DERVIN, P., MARDON, J. P. & ENGLANDER, M. 1979. La diffraction neutronique appliquee a l'etude de l'orientation preferentielle de reseau dans les quartzites. *In*: NICOLAS, A., DAROT, M. & WILLAIME, C. (eds) *Mecanismes de Deformation des Mineraux et des Roches*. Bulletin de Mineralogie, **102**, 225–231.

BUNGE, H. J. 1982. *Texture analysis in Material Science – Mathematical methods*. Butterworths, London.

BUNGE, H. J. & ESLING, C. 1982. *Quantitative Texture Analysis*. DGM, Germany.

BUNGE, H. J., SIEGESMUND, S. & WEBER, K. 1994. *Textures of Geological Materials*. Oberusel. 399.

BUNGE, H. J., WENK, H. R. & PANNETIER, J. 1982. Neutron diffraction texture analysis using a 2q position sensitive detector. *Textures and Microstructures*, **5**, 153–170.

BUSSY, F., VENTURINI, G., HUNZIKER, J. & MARTINOTTI, G. 1998. U-Pb ages of magmatic rocks of the western Austroalpine Dent-Blanche-Sesia Unit. *Schweizerische Mineralogische und Petrographische Mitteilungen*, **78**, 163–168.

CHATEIGNER, D., HEDEGAARD, C. & WENK, H. R. 2000. Mollusc shell microstructures and crystallographic textures. *In*: LEISS, B., ULLEMEYER, K. & WEBER, K. (eds) *Journal of Structural Geology. Special Issue: Textures and physical properties of rocks*, **22**, 1723–1735.

CHATEIGNER, D., WENK, H. R. & PERNET, M. 1999. Orientation distributions of low symmetry polyphase materials using neutron diffraction data: application to a rock composed of quartz, biotite and feldspar. *Textures and Microstructures*, **33**, 35–43.

COLBY, J. W. 1968. Quantitative microprobe analysis of thin insulating films. *Advances in X-Ray Analysis*, **11**, 287–305.

COMODI, P., MELLINI, M., UNGARETTI, L. & ZANAZZI, P. F. 1991. Compressibility and high pressure structure refinement of tremolite, pargasite and glaucophane. *European Journal of Mineralogy*, **3**, 485–499.

COMPAGNONI, R. 1977. The Sesia-Lanzo zone: high-pressure low-temperature metamorphism in the Austroalpine continental margin. *Rendiconti della Società Italiana di Mineralogia e Petrologia*, **33**, 335–374.

CUMBEST, R. J., DRURY, M. R., VAN ROERMUND, H. L. M. & SIMPSON, C. 1989. Dynamic recrystallization and chemical evolution of clinoamphibole from Senja Norway. *Contributions to Mineralogy and Petrology*, **101**, 339–349.

DAL PIAZ, G. V., VENTURELLI, G. & SCOLARI, A. 1979. Calc-alkaline to ultrapotassic post-collisional volcanic activity in the internal northwestern Alps. *Memorie della Società Geoligica Italiana, Padova*, **32**, 4–15.

DE CAPITANI, L., POTENZA FIORENTINI, M., MARCHI, A. & SELLA, M. 1979. Chemical and Tectonic contributions to the age and petrology of the Canavese and Sesia-Lanzo 'porphyrites'. *Atti Società Italiana di Scienze Naturali*, **120**, 151–179.

DOLLINGER, G. & BLACIC, J. D. 1975. Deformation mechanisms in experimentally and naturally deformed amphiboles. *Earth and Planetary Science Letters*, **26**, 409–416.

DUCHENE, S., BLICHERT, T. J., LUAIS, B., TELOUK, P., LARDEAUX, J. M. & ALBAREDE, F. 1997. The Lu-Hf dating of garnets and the ages of the Alpine high-pressure metamorphism. *Nature*, **387**, 586–589.

GAPAIS, D. & BRUN, J. P. 1981. A comparison of mineral grain fabrics and finite strain in amphibolites from eastern Finland. *Canadian Journal of Earth Sciences*, **18**, 995–1003.

GAPAIS, D. & COBBOLD, P. R. 1987. Slip system domains: 2, Kinematic aspects of fabric development in polycrystalline aggregates. *Tectonophysics*, **138**, 289–309.

GHOSE, S., KERSTEN, M., LANGER, K., ROSSI, G. & UNGARETTI, L. 1986. Crystal field spectra and Jahn Teller effect of Mn (super 34) in clinopyroxene and clinoamphiboles from India. *Physics and Chemistry of Minerals*, **13**, 291–305.

GOSSO, G. 1977. Metamorphic evolution and fold history in the eclogite micaschists of the upper Gressoney valley (Sesia-Lanzo zone, Western Alps). *Rendiconti della Società Italiana di Mineralogia e Petrologia*, **33**, 389–407.

HAWTORN, F. C., DELLA VENTURA, G., ROBERT, J.-L., WELCH, M. D., RAUDSEPP, M. & JENKINS, D. M. 1997. A Rietveld and infrared study of synthetic amphibole along the potassium-richterite tremolite join. *American Mineralogist*, **82**, 708–716.

HELMING, K. 1991. Minimal pole figures ranges for quantitative texture analysis. *Textures and Microstructures*, **19**, 45–54.

HOWARD, S. A. & PRESTON, K. D. 1989. Profile fitting of powder diffraction patterns. *Reviews in Mineralogy*, **20**, 217–275.

ILDEFONSE, B., LARDEAUX, J. M. & CARON, J. M. 1990. The behavior of shape preferred orientations in the metamorphic rocks: amphiboles and jadeites from the Monte Mucrone Area (Sesia-Lanzo Zone, Italian Western Alps). *Journal of Structural Geology*, **12**, 1005–1011.

INEL 1986. *Goman*. World Wide Web Address: http://www.valcofim.fr/inel/

INGER, S., RAMSBOTHAM, W., CLIFF, R. A. & REX, D. C. 1996. Metamorphic evolution of the Sesia–Lanzo Zone, Western Alps: time constraints from multi-system geochronology. *Contribution to Mineralogy and Petrology*, **126**, 152–168.

Ok?

KERN, H. & FAKHIMI, M. 1975. Effect of fabric anisotropy on compressional wave propagation in various metamorphic rocks for the range 20–700°C at 2 kbars. *Tectonophysics*, **28**, 227–244.

KOCKS, F., TOME, C. & WENK, R. 1998. *Texture and Anisotropy*. Cambridge University Press, Cambridge.

KRUHL, J. H. & HUNTEMANN, T. 1991. The structural state of the former lower continental crust in Calabria. *Geologische Rundschau*, **80**, 289–302.

LARDEAUX, J. M. & SPALLA, M. I. 1991. From granulites to eclogites in the Sesia zone (Italian Western Alps): a record of the opening and closure of the Piedmont ocean. *Journal of Metamamorphic Geology*, **9**, 35–59.

LAW, R. D. 1990. Crustallographic fabrics: a selective review of their applications to research in structural geology. *In*: KNIPE, R. J. & RUTTER, E. H. (eds) *Deformation Mechanisms, Rheology and Tectonics*, Geological Society, London, Special Publications, **54**, 335–352.

LEISS, B., ULLEMEYER, K. & WEBER, K. 2000. *Textures and Physical Properties of Rocks*. Pergamon, Oxford, International.

LUTTEROTTI, L., MATTHIES, S. & WENK, H. R. 1999. MAUD (Material Analysis Using Diffraction): a user friendly Java program for Rietveld Texture Analysis and more. *In*: SZPUNAR, J. A. (ed.) *Proceedings of the Twelfth International Conference on Textures of Materials (ICOTOM-12)*, **2**, 1599.

LUTTEROTTI, L., MATTHIES, S., WENK, H. R., SCHULTZ, A. J. & RICHARDSON, J. J. W. 1997. Combined texture and structure analysis of deformed limestone from time-of-flight neutron diffraction spectra. *Journal of Applied Physics*, **81**, 594–600.

MAINPRICE, D. & NICOLAS, A. 1989. Development of shape and lattice preferred orientations: Application to the seismic anisotropy of the lower crust. *Journal of Structural Geology*, **11**, 391–398.

MATTHIES, S. 1991. On the principle of conditional ghost correction and its realization in existing correction concepts. *Textures and Microstructures*, **14–18**, 1–12.

MATTHIES, S. & VINEL, G. W. 1982. On the reproduction of the orientation distribution function of textured samples from reduced pole figures using the concept of ghost correction. *Physica Status Solidi (a)*, **112**, K111–114.

MATTHIES, S., LUTTEROTTI, L. & WENK, H. R. 1997. Advances in texture analysis from diffraction spectra. *Journal of Applied Crystallography*, **30**, 31–42.

MORRISON, S. D. J. 1976. Transmission electron microscopy of experimentally deformed hornblende. *American Mineralogist*, **61**, 272–280.

NICOLAS, A. & POIRIER, J. P. 1976. *Crystalline Plasticity and Solid State Flow in Metamorphic Rocks*. Wiley, London.

NYMAN, M. W., LAW, R. D. & SMELIK, E. A. 1992. Cataclastic deformation for the development of core mantle structures in amphibole. *Geology*, **20**, 455–458.

PASSCHIER, C. W., URAI, J. L., VAN LOON, J. & WILLIMAS, P. F. 1981. Structural geology of the Central Sesia-Lanzo Zone. *Geologie en Mijnbouw*, **60**, 497–507.

POGNANTE, U., COMPAGNONI, R. & GOSSO, G. 1980. Micro-mesostructural relationships in the continental eclogitic rocks of the Sesia-Lanzo zone: a record of a subduction cycle (Italian Western Alps). *Rendiconti della Società Italiana di Mineralogia e Petrologia*, **36**, 169–186.

PRIOR, D. J., BOYLE, A. P., *ET AL.* 1999. The application of electron backscatter diffraction and orientation contrast imaging in the SEM to textural problems in rocks. *American Mineralogist*, **84**, 1741–1759.

REYNARD, B., GILLET, P. & WILLAIME, C. 1989. Deformation mechanisms in naturally deformed glaucophanes; a TEM and HREM study. *European Journal of Mineralogy*, **1**, 611–624.

RICOTE, J. & CHATEIGNER, D. 1999. Quantitative texture analysis applied to the study of preferential orientations in ferroelectric thin films. *Boletin Sociedad Española de Ceramica y Vidrio*, **38**, 587–591.

RIECKER, R. E. & ROONEY, T. P. 1969. Water-induced weakening of hornblende and amphibolite. *Nature*, **224**, 1299.

ROONEY, T. P., RIECKER, R. E. & ROSS, M. 1970. Deformation twins in hornblende. *Science*, **169**, 173–175.

RUBATTO, D., GEBAUER, D. & COMPAGNONI, R. 1999. Dating of eclogite-facies zircons; the age of Alpine metamorphism in the Sesia-Lanzo Zone (Western Alps). *Earth and Planetary Science Letters*, **167**, 141–158.

RUFFET, G., GRUAU, G., BALLEVRE, M., FERAUD, G. & PHILIPPOT, P. 1997. Rb-Sr and (super 40) Ar-(super 39) Ar laser probe dating of high-pressure phengites from the Sesia Zone (Western Alps); underscoring of excess argon and new age constraints on the high-pressure metamorphism. *Chemical Geology*, **141**, 1–18.

SCHWERDTNER, W. M. 1964. Preferred orientation of hornblende in a banded hornblende gneiss. *American Journal of Science*, **262**, 1212–1229.

SCHWERDTNER, W. M., SHEEHAN, P. M. & RUCKLIDGE, J. C. 1971. Variation in degree of hornblende grain alignment within two boudinage structures. *Canadian Journal of Earth Sciences*, **8**, 144–149.

SHELLEY, D. 1993. *Igneous and Metamorphic Rocks under the Microscope*. Chapman and Hall, London.

SHELLEY, D. 1994. Spider texture and amphibole preferred orientation. *Journal of Structural Geology*, **16**, 709–717.

SHELLEY, D. 1995. Asymmetric shape preferred orientation as shear-sense indicators. *Journal of Structural Geology*, **17**, 509–518.

SIEGESMUND, S., HELMING, K. & KRUSE, R. 1994. Complete texture analysis of a deformed amphibolite: comparison between neutron, diffraction and U-stage data. *Journal of Structural Geology*, **16**, 131–142.

SKROTZKI, W. 1990. Microstructure in hornblende of a mylonite amphibolite. *In*: KNIPE, R. J. & RUTTER, E. H. (eds) *Deformation Mechanisms, Rheology and Tectonics*, Geological Society, London, Special Publications, **54**, 321–325.

SKROTZKI, W. 1992. Defect structures and deformation mechanisms in naturally deformed hornblende. Physica Status Solidi (a), 131, 605–624.

SMYTH, J. R., DYAR, M. D., MAY, H. M., BRICKER, O. P. & ACKER, J. G. 1981. Crystal structure refinement and Moessbauer spectroscopy of an ordered triclinic clinochlore. *Clays and Clay Min.*, **29**, 544–550.

SPALLA, M. I., DE MARIA, L., GOSSO, G., MILETTO, M. & POGNANTE, U. 1983. Deformazione e metamorfismo della Zona Sesia - Lanzo meridionale al contatto con la falda piemontese e con il massiccio di Lanzo, Alpi occidentali. *Memorie della Società Geoligica Italiana, Padova*, **26**, 499–514.

STÜNITZ, H. 1989. *Partitioning of Metamorphism and Deformation in the Boundary Region of the 'Seconda Zona Diorito-Kinzigitica', Sesia Zone, Western Alps.* PhD Thesis, ETH, Zurich.

ULLEMEYER, K., BRAUN, G., DAHMS, M., KRUHL, J. H., OLESEN, N. O. & SIEGESMUND, S. 2000. Texture analysis of a muscovite-bearing quartzite; a comparison of some currently used techniques. *In*: LEISS, B., ULLEMEYER, K. & WEBER, K. (eds) *Textures and Physical Properties of Rocks.*

VENTURINI, G., MARTINOTTI, G. & HUNZIKER, J. C. 1991. The protoliths of the 'Eclogitic Micaschists in the lower Aosta Valley (Sesia-Lanzo zone, Western Alps). *Memorie della Società Geoligica Italiana*, **43**, 347–359.

WENK, H. R. 1985. *Preferred orientation in deformed metals and rocks; an introduction to modern texture analysis.* Academic Press, Orlando, FL, United States.

WENK, H. R. 1998. Plasticity modeling in minerals and rocks. *In*: KOCKS, U. F. TOMÉ, C. N. & WENK, H. R. (eds) *Texture and Anisotropy: Preferred Orientations in Polycrystals and their Effect on Material Properties*, 676.

WENK, H. R., CONT, L., LUTTEROTTI, L., RATSCHBACHER, L. & RICHARDSON, J. 2001. Rietveld texture analysis of Dabie Shan eclogite from TOF neutron diffraction spectra. *Journal of Applied Crystallography*, **34**, 442–453.

WENK, H. R., KERN, H., SCHAFER, W. & WILL, G. 1984. Comparison of x-ray and neutron diffraction in textures analysis of carbonate rocks. *Journal of Structural Geology*, **6**, 687–692.

WENK, H. R., MATTHIES, S., DONOVAN, J. & CHATEIGNER, D. 1998. Beartex: a Windows-based program system for quantitative texture analysis. *Journal of Applied Crystallography*, **31**, 262–269.

WENK, H. R., MATTHIES, S., HEMLEY, R. J., MAO, H. K. & SHU, J. 2000. The plastic deformation of iron at pressures of the Earth's inner core. *Nature*, **45**, 1044–1047.

WILLIAMS, P. F. & COMPAGNONI, R. 1983. Deformation and metamorphism in the Bard area of the Sesia-Lanzo zone, Western Alps, during subductionand uplift. *Journal of Metamamorphic Geology*, **1**, 117–140.